Molecular and Cellular Biochemistry (2021) 476:959–969
https://doi.org/10.1007/s11010-020-03963-9

Androgen depletion alters the diurnal patterns to signals that regulate autophagy in the limb skeletal muscle

Michael L. Rossetti[1] · Robert J. Tomko Jr[2] · Bradley S. Gordon[1,3]

Received: 19 August 2020 / Accepted: 23 October 2020 / Published online: 31 October 2020

Abstract

Hypogonadism contributes to limb skeletal muscle atrophy by increasing rates of muscle protein breakdown. Androgen depletion increases markers of the autophagy protein breakdown pathway in the limb muscle that persist throughout the diurnal cycle. However, the regulatory signals underpinning the increase in autophagy markers remain ill-defined. The purpose of this study was to characterize changes to autophagy regulatory signals in the limb skeletal muscle following androgen depletion. Male mice were subjected to a castration surgery or a sham surgery as a control. Seven weeks post-surgery, a subset of mice from each group was sacrificed every 4 hr over a 24 hr period. Protein and mRNA from the Tibialis Anterior (TA) were subjected to Western blot and RT-PCR. Consistent with an overall increase in autophagy, the phosphorylation pattern of Uncoordinated Like Kinase 1 (ULK1) (Ser555) was elevated throughout the diurnal cycle in the TA of castrated mice. Factors that induce the progression of autophagy were also increased in the TA following androgen depletion including an increase in the phosphorylation of c-Jun N-terminal Kinase (JNK) (Thr183/Tyr185) and an increase in the ratio of BCL-2 Associated X (BAX) to B-cell lymphoma 2 (BCL-2). Moreover, we observed an increase in the protein expression pattern of p53 and the mRNA of the p53 target genes Cyclin-Dependent Kinase Inhibitor 1A (*p21*) and Growth Arrest and DNA Damage Alpha (*Gadd45a*), which are known to increase autophagy and induce muscle atrophy. These data characterize novel changes to autophagy regulatory signals in the limb skeletal muscle following androgen deprivation.

Keywords Muscle atrophy · Hypogonadism · Protein degradation

Introduction

Maintaining a critical amount of skeletal muscle mass is important to sustain physical function and reduce the risk of morbidity and mortality [1–4]. In males, testicular derived androgens are a key factor regulating muscle mass [5–7]. This mode of regulation is critical when endogenous production is compromised (termed hypogonadism) as muscle mass is decreased [8–10]. Atrophy of the limb muscles during hypogonadism is particularly important as they comprise most of the total muscle mass [11], and they are the primary contributors to physical function. Although androgen replacement therapy blunts limb muscle atrophy in hypogonadal males in part by reducing rates of skeletal muscle protein breakdown to normal levels [9], this treatment has been associated with undesirable side effects (e.g., malignant tumor growth) [12–15]. This requires a full understanding of the reasons underpinning the elevated rates of muscle protein breakdown in the limb muscle so that clinicians can safely and effectively treat limb muscle atrophy during hypogonadism.

We and others have shown that markers of the autophagy protein breakdown process are elevated in the atrophied limb muscle following androgen depletion [16–20]. These markers of autophagy were elevated across the diurnal cycle [18], supporting a leading role for this degradative process in the limb muscle atrophy during hypogonadism. Autophagy is the process of bulk clearance of misfolded/aggregate proteins and dysfunctional/damaged organelles

✉ Bradley S. Gordon
bsgordon@fsu.edu

[1] Department of Nutrition, Food and Exercise Science, Florida State University, 600 W. Cottage Avenue, Tallahassee, FL 32306, USA

[2] Department of Biomedical Sciences, Florida State University College of Medicine, 115 W Call Street, Tallahassee, FL 32304, USA

[3] Institute of Sports Sciences and Medicine, Florida State University, 600 W. Cottage Ave, Tallahassee, FL 32306, USA

(e.g., mitochondria via mitophagy) [21]. Upon activation of autophagy, proteins and organelles are delivered to the lysosome via a double membrane bound vesicle known as the autophagosome, ultimately resulting in proteolytic degradation of the cargo [21]. Various external stimuli (e.g., nutrients & exercise) activate/repress a number of cellular signaling events that regulate the initiation and progression of autophagy [19, 22–27]. For example, activation of uncoordinated 51 like kinase 1 (ULK1) recruits the PI3k class III complex containing BECLIN1 (a.k.a. ATG6), which initiates formation and maturation of a double membrane structure called a phagophore (immature autophagosome) [21]. When the phagophore nears maturity, Microtubule Associated Protein 1 Light Chain 3 Beta (LC3B) is lipidated to allow closure of the autophagosome and subsequent delivery of the cargo to the lysosome [21].

Despite evidence that autophagy is overactive across the diurnal cycle in the limb muscle following androgen depletion, the regulatory signals that stimulate overactivation remain poorly defined. Thus, the purpose of this study was to characterize the diurnal changes to autophagy regulatory signals in the limb muscle following androgen depletion. Using a novel analytical approach, we provide evidence that androgen depletion alters the diurnal patterns of key autophagy regulatory signals in the limb muscle, including those that are known to induce limb muscle atrophy. These findings represent a significant step toward mapping the pathways that link hypogonadism to limb muscle atrophy.

Materials and methods

Animals, castration surgery, and experimental design

The muscle samples used in the current study were generated from a previous study conducted by our laboratory[18]. Briefly, physically mature male, C57Bl/6NHsd mice (14 weeks of age) were randomized into two groups of equal body weight. One group was subjected to a castration surgery to effectively stop testicular androgen production, while the other group was subjected to a sham surgery where the testicles were left intact. Animals recovered for seven weeks prior to sacrifice. At sacrifice, the TA muscles were harvested from a subset of mice from each group (sham or castrated) every 4 hr, starting at the onset of the dark cycle (1900 hr). Animals were allowed *ad libitum* food and water throughout data collection, and physical activity was not monitored or regulated. Our previous work suggests that autophagy markers are elevated independent of both nutrient consumption and/or activity [16, 17, 19], suggesting that changes in nutrient consumption and/or physical activity are not likely altering the autophagy regulatory processes following androgen depletion. For animals sacrificed during the dark cycle (1900–0300 hr), the mouse cage was placed into an opaque Tupperware container for transport to the surgical suite to prevent light exposure. In the surgical suite, mice were anesthetized with isoflurane (~3%) and then euthanized via cervical dislocation under dim red light. Lights were then turned on and the TA muscles were harvested and frozen in liquid nitrogen. The efficacy of the castration surgery was supported by a ~16% decrease in mean TA mass (50.98 mg vs. 42.6 mg) and a substantial decrease in the mean mass of the androgen-sensitive seminal vesicle (364.4 mg vs. 11.0 mg) in sham and castrated mice, respectively [18].

RNA extraction, cDNA synthesis, and RT-PCR

TA muscles (~20 mg) were homogenized in 600 µl of Zymo Tri Reagent (Irvine, CA), and RNA was isolated using a Zymo RNA Miniprep extraction kit (cat. #R2071) with on column DNase treatment (Irvine, CA). RNA quantity was determined spectrophotometrically by the 260-to-280 nm ratio. Following this, cDNA was synthesized from 1.5 µg of total RNA using a High Capacity cDNA Reverse Transcription Kit (Thermo Fisher Scientific, Waltham, MA). RT-PCR was conducted on a QuantStudio3 (Thermo Fisher Scientific) RT-PCR thermal cycler using PowerUp Sybr Green Master Mix (Thermo Fisher Scientific). The conditions for RT-PCR with Sybr Green included an initial 2 min at 50 °C and 2 min at 95 °C, followed by 40 cycles which included a 15 sec denature step at 95 °C, a 15 sec annealing step at 55 °C, and a 1 min extension step at 72 °C within each cycle. A melt curve analysis was performed for each primer pair to ensure that a single product was efficiently amplified, and the product sizes for each primer pair were verified via agarose gel electrophoresis prior to experimentation. Relative expression levels of all genes were normalized using the delta Ct method. Ribosomal Protein Lateral Stalk Subunit P0 (*Rplp0*) was used as the internal control as *Rplp0* expression was not affected by either time or castration. Primer sequences for all Sybr Green RT-PCR reactions are listed in Table 1.

Western blot analysis

Western blotting was conducted as previously described with slight modifications [18]. Whole-muscle protein from the TA was extracted via glass on glass homogenization in 10 volumes of buffer (10 µl/mg) consisting of 50 mM HEPES (pH 7.4), 0.1% Triton-X 100, 4 mM EGTA, 10 mM EDTA, 15 mM Na4P2O7, 100 mM β-glycerophosphate, 25 mM NaF, 5 mM Na3VO4, and 10 µl/ml protease inhibitor cocktail (cat. no. P8340, Sigma-Aldrich). The extract was centrifuged for 10 min at 10,000 g at 4 °C, and the

Table 1 Primer sequences for RT-PCR using Sybr Green

Gene symbol	Forward (5′-3′)	Reverse (5′-3′)	Amplicon size (BP)
Atf4	TCGATGCTCTGTTTCGAATG	GGCAACCTGGTCGACTTTTA	179
Bax	CGAGCTGATCAGAACCATCAT	GAGTCCAGCCACAAAGA	154
Bcl-2	TGGTGGAGGAACTCTTCAGG	CAGATGCCGGTTCAGGTACT	158
Beclin1	TCACCATCCAGGAACTCACA	CCCCGATCAGAGTGAAGCTA	192
Gadd45a	CAGAGCAGAAGACCGAAAGG	GCAGGCACAGTACCACGTTA	150
p21	ACGGTGGAACTTTGACTTCG	CAGGGCAGAGGAAGTACTGG	160
p53	CACAGCGTGGTGGTACCTTA	CAGGCACAAACACGAACCTC	191
Redd1	TGGTGCCCACCTTTCAGTTG	GTCAGGGACTGGCTGTAACC	121
Rplp0	CAACCCAGCTCTGGAGAAAC	GTTCTGAGCTGGCACAGTGA	169
Tfeb	AACAGTGCTCCCAACAGTCC	CATCTGCATCTCAGGGTTGA	132

Bradford method was used to quantify the soluble protein content in the supernatant fraction. After quantification, all samples were diluted to the same concentration in 2X Laemmli buffer. Samples were fractionated on 4–20% Bio-Rad Criterion precast gels (Hercules, CA) and transferred to PVDF membranes. Effective transfer and equal protein loading were verified by Ponceau-S staining. Membranes were then blocked with 5% nonfat dried milk in Tris-buffered saline (TBS) + 0.1% Tween 20 (TBST). Membranes were then incubated overnight at 4 °C with antibodies against mTOR (Ser2481) (cat. #2974), mTOR (cat. #2972), BAX (cat. #14796), BCL-2 (cat. #3498), BECLIN1 (cat. #3738), p53 (cat. #2524), p38 (Thr180/Tyr182) (cat. #9211), p38 (cat. #9212), JNK (Thr183/Tyr185) (cat. #9251), total JNK (cat. #9252), 4E-BP1 (Ser65) (cat. #9451), AMPKα (Thr172) (cat. #2531), total AMPKα (cat. #2532), PP2Ac (cat. #2259), Histone H2B (cat. #8135), ULK1 (Ser555) (cat. #5869), and ULK1 (Ser757) (cat. #6888), and total ULK1 (cat. #8054), which were all obtained from Cell Signaling Technology (Danvers, MA). Antibodies against GAPDH (cat. #sc-32233) were obtained from Santa Cruz Biotechnology (Dallas TX). Antibodies against total 4E-BP1 were custom made by Bethyl Laboratories (Montgomery, TX) and kindly provided by Dr. Scot Kimball (Pennsylvania State University College of Medicine, Hershey, PA). The next morning, membranes were incubated with the appropriate secondary antibodies (Bethyl Laboratories, cat. #A120-101P or A90-116P, Montgomery, TX), and the antigen-antibody complex was visualized by enhanced chemiluminescence using Clarity reagent (Bio-Rad) on a Bio-Rad ChemiDoc Touch imaging system. Pixel density from all blots were quantified using Image J software (NIH, Bethesda, MD), and expression of total protein was normalized to a predefined region around the 45 kD band of the Ponceau-S stained membrane. Because of the logistical limitations for Western blotting a single data set containing 36 samples, and a small N per group per time point, we used a modified analysis previously conducted by us and others [18, 28]. For this modified analysis, an equal amount of protein from the three samples within a group (sham or castrated) at each circadian timepoint was pooled together prior to Western blot analysis. This allowed us to generate diurnal protein expression patterns for each group on the same gel. Differences in the protein expression patterns between groups were initially detected visually if the quantified pixel intensity of the pooled samples appeared to differ across ≥3 consecutive time points. If an expression pattern was visually observed, differences in the mean pixel intensity obtained from the ≥3 time points was assessed statistically by Student's *t*-test. The validity of this method to assess diurnal patterns is supported by our previous work and others where it properly identified the expected diurnal patterns of various proteins and regulatory signals in the TA muscle and liver of wild type animals [18, 28].

Cytosolic/nuclear fractionation

Whole gastrocnemius muscle samples were homogenized using glass on glass in 10 volumes (10 µl/mg tissue) of buffer (referred here after as buffer A) consisting of 10 mM NaCl, 1.5 mM $MgCl_2$, 20 mM HEPES, 20% glycerol, 0.1% Triton-X 100, 1 mM DTT, and 10 µl/ml protease inhibitor cocktail (Sigma-Aldrich #P8340, St. Louis, MO). Samples were centrifuged for 5 min at 2400 *x g* at 4 °C. The supernatant was collected and saved as the cytosolic enriched fraction. This fraction was further centrifuged three times, each at 5-min/3500 *x g*/4 °C, to pellet and remove any remaining non-cytosolic material. The pellet containing the nuclear-enriched fraction was then gently washed three times in buffer A. Between each wash, the nuclear pellet was centrifuged for 5 min at 2400 *x g* at 4 °C. The final nuclear pellet was then suspended in 400 µl of the protein extraction buffer described in the Western blot analysis section. The sample was then centrifuged for 15 min at 21,000 *x g* at 4 °C. The supernatant was collected and saved as the nuclear-enriched fraction. The protein content of each fraction was quantified

by the Bradford method, and equal quantities of protein were diluted into 2X Laemmli buffer. At each circadian time point, an equal amount of protein from each fraction from the three samples within a group (sham or castrated) was pooled together prior to Western blot analysis.

Statistical analysis

Protein expression from pooled samples are presented as a single value at each time point for each condition (sham or castrated). All gene expression data are presented as mean ± SEM. Two-way ANOVA was used to assess changes in mRNA across the sampling period using castration and time as the two factors. No interactions were observed, thus only main effects are reported. Differences in protein expression patterns from ≥3 consecutive time points were assessed by Student's *t*-test to estimate differences in expression patterns. All analysis was performed using GraphPad Prism Software (La Jolla, CA). Significance for all analysis was set at $P \leq 0.05$.

Results

Signals that regulate autophagy initiation are increased in the limb muscle following androgen depletion

We previously showed that markers of macroautophagy (e.g., LC3B & p62) and microautophagy (e.g., Pink1/Parkin, BNIP3) were increased across the diurnal cycle in the atrophied TA of mice following androgen depletion, with the greatest increase occurring in the dark cycle (Circadian Time 12-24/0) [18]. This differed from the TA of eugonadal sham mice as autophagy markers were suppressed during the dark cycle (Circadian Time 12-24/0) and elevated only during the light cycle (Circadian Time 24/0-8) [18]. The diurnal changes in autophagy markers previously described in the TA muscles of those sham and castrated mice are summarized in Fig. 1a. The present study used the extracts from those same muscles to investigate changes to the diurnal autophagy regulatory signals. Autophagy can be initiated largely through changes in the phosphorylation of ULK1 [23, 24]. For instance, the mechanistic target of rapamycin in complex 1 (mTORC1) phosphorylates ULK1 on Ser757 to inhibit activation, while kinases such as 5′ AMP Activated Protein Kinase (AMPK) phosphorylate ULK1 on Ser555 to induce activation [23, 24]. In the TA of sham mice, the phosphorylation pattern of ULK1 (Ser757) was inversely related to the autophagy patterns previously reported in those muscles (Fig. 1b, i). The ULK1 (Ser757) pattern in the TA of castrated mice was mostly similar to the pattern observed in sham mice (Fig. 1b, i). The phosphorylation patterns of mTOR (Ser2481) and the mTORC1 target, 4E-BP1 (Ser65), were similar to that observed for ULK1 (Ser757), with slight elevations occurring in the TA of castrated mice (Fig. 1c, d, i).

In contrast to what was observed for ULK1 Ser757, the phosphorylation pattern for ULK1 Ser555 peaked in the TA of sham mice when autophagy markers exhibited their greatest suppression (CT 12-24/0) (Fig. 1e, i). While this was unexpected, the phosphorylation pattern (and presumed activation) of AMPK (Thr172) in the TA of sham mice was nearly identical to that of ULK1 (Ser555) (Fig. 1f, i), implying a certain level of autophagy may normally persist throughout the diurnal cycle, and this may be mediated, at least in part, by AMPK. In contrast, the phosphorylation pattern of ULK1 (Ser555) was elevated throughout the entire sampling period in the TA of castrated mice (Fig. 1e, i). However, the ULK1 (Ser555) pattern in the TA of castrated mice did not correspond with the pattern of AMPK (Thr172), as it was actually slightly lower than sham values throughout much of the sampling period (Fig. 1f, i). The Ser555 residue is within the *RXXS* consensus sequence, which can also be phosphorylated by the p38 MAPK in skeletal muscle to induce autophagy [29, 30]. However, the p38 phosphorylation pattern was not different between groups (Fig. 1g, i). The phosphatase(s) that target the Ser555 residue on ULK1 are ill-defined, but Protein Phosphatase 2A (PP2A) is known to dephosphorylate other residues on ULK1 to promote autophagy in an mTORC1-independent manner [31]. This was an unlikely source of activation as the expression pattern of the catalytic subunit of PP2A (PP2Ac) was slightly lower in the TA of castrated mice (Fig. 1h, i). Thus, the kinases/phosphatases responsible for activating ULK1 following androgen depletion remain ill-defined.

Expression patterns of key regulatory components involved with BECLIN1 activation are altered in the limb muscle following androgen depletion

BECLIN1 is a component of the PI3K class complex that promotes autophagosome formation/maturation [21]. BECLIN1 activity is inhibited by interaction with B-cell lymphoma 2 (BCL-2) [32], which can occur through changes in BCL-2 expression, changes in expression of other BCL-2 family proteins, or BCL-2 phosphorylation [33–36]. For instance, the interaction of BCL-2 and BECLIN1 and subsequent activation state of BECLIN1 can be altered through phosphorylation by active c-Jun N-terminal Kinase (JNK) [34]. In addition, BCL-2 can also be inactivated by increasing expression of the pro apoptotic protein, BCL-2 Associated X (BAX) [35, 36]. Interestingly, there was no overt diurnal pattern for BECLIN1 protein in sham animals, and this pattern was only minimally affected by androgen depletion (Fig. 2a, g). In the TA of sham mice, the expression

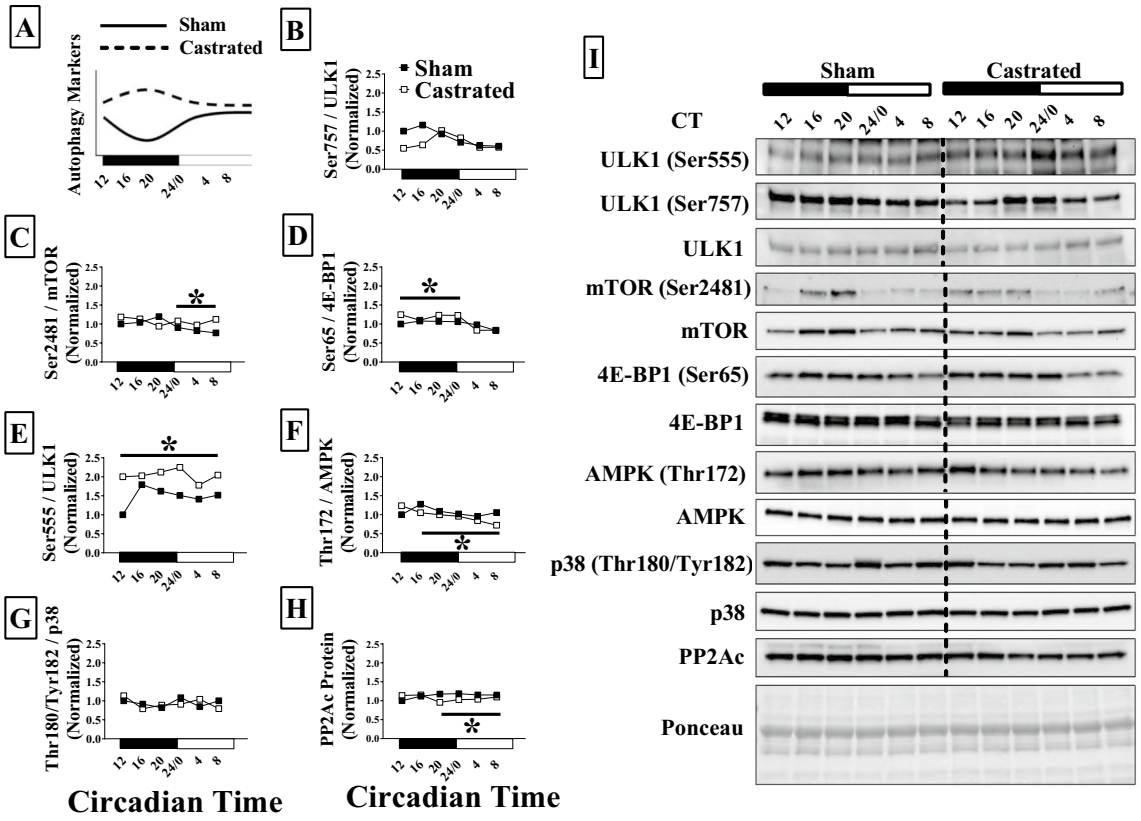

Fig. 1 The diurnal pattern of factors regulating initiation of autophagy in the TA following androgen depletion. (**a**) Summary of previously identified castration-induced changes in diurnal autophagy markers in the TA muscles analyzed in the present study. The diurnal pattern of phosphorylated to total protein for (**b**) ULK1 (Ser757), (**c**) mTOR (Ser2481), (**d**) 4E-BP1 (Ser65), (**e**) ULK1 (Ser555), (**f**) AMPK (Thr172), (**g**) p38 (Thr180/Tyr182) were determined in the TA of sham and castrated mice by Western blot analysis. (**h**) The diurnal pattern of PP2Ac protein was determined by Western blot analysis. (**i**) Western blot. Dotted line on blot is used to visually separate sham and castrated groups. For Western blot analysis, an equal amount of protein was pooled together from each sample within a group ($N=3$) at each time point for analysis. If a visual difference in the expression patterns was observed across three or more consecutive time points, differences in the mean pixel intensity obtained from those time points were assessed statistically. Student's *t*-test was used to assess differences in pixel intensity of ≥3 consecutive time points. $N=3$ pooled samples/group/time point. *Significant difference from ≥3 consecutive time points under the solid black line. $p \leq 0.05$ for all analysis

patterns for BCL-2 and the ratio of BCL-2 to BECLIN1 were inversely related to the diurnal autophagy pattern (Figs. 1a and 2b, c, g). Ironically, the induction of autophagy markers in the TA of castrated mice from CT 24/0 to 8 (Fig. 1a) coincided with increased patterns for both BCL-2 and the ratio of BCL-2 to BECLIN1 (Fig. 2b, c, g), implying a minimal role for changes in expression of BCL-2 in the autophagy induction at those time points. While the phosphorylation pattern (and presumed activation) of JNK (Thr183/Tyr185) was directly related to autophagy markers in the TA of sham mice (Figs. 1a and 2d, g), it was elevated from Circadian Time 12–20 following androgen depletion (Fig. 2d, g), implying a potential role for this kinase to inhibit BCL-2 at those sampling time points.

In the TA of sham mice, the expression patterns of BAX and the ratio of BAX to BCL-2 were directly related to diurnal changes in autophagy markers (Figs. 1a and 2e, f, g). Alternatively, the expression pattern of BAX protein and the ratio of BAX to BCL-2 were elevated across much of the diurnal cycle following androgen depletion (Fig. 2). These observed changes in BECLIN1, BCL-2, and BAX proteins following androgen depletion were not likely mediated at the transcriptional level as there were no differences in the relative transcript abundances of each gene (Fig. 3a–c). Together, these data suggest that changes to the BCL-2/BECLIN1 regulatory process via JNK and/or BAX coincide with induction of diurnal autophagy markers following androgen depletion.

Androgen depletion increases markers of p53 pathway activation in the limb skeletal muscle

In addition to the previously described modes of autophagy regulation, other pathways also induce autophagy, though

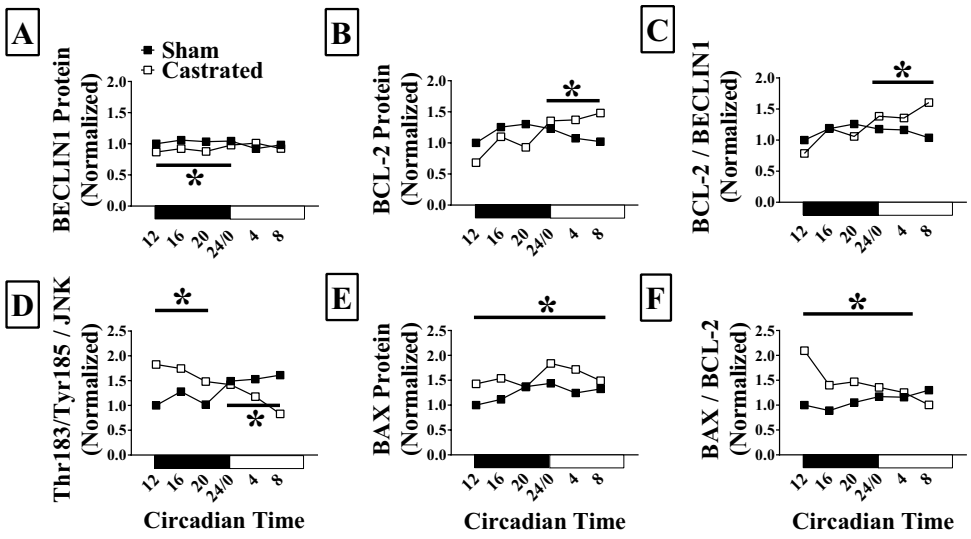

Fig. 2 The diurnal pattern of factors regulating BECLIN1 activity in the TA following androgen depletion. The circadian expression patterns of (**a**) BECLIN1, (**b**) BCL-2, (**c**) the BCL-2 to BECLIN1 ratio, (**d**) the phosphorylated to total protein ratio of JNK (Thr183/Tyr185), (**e**) BAX, and (**f**) the BAX to BCL-2 ratio were assessed by Western blot analysis. (**g**) Western blot. Dotted line on blot is used to visually separate sham and castrated groups. For Western blot analysis, an equal amount of protein was pooled together from each sample within a group ($N=3$) at each time point for analysis. If a visual difference in the expression patterns was observed across three or more consecutive time points, differences in the mean pixel intensity obtained from those time points were assessed statistically. Student's *t*-test was used to assess differences in pixel intensity of ≥3 consecutive time points. $N=3$ pooled samples/group/time point. * Significant difference from ≥3 consecutive time points under the solid black line. $p \leq 0.05$ for all analysis

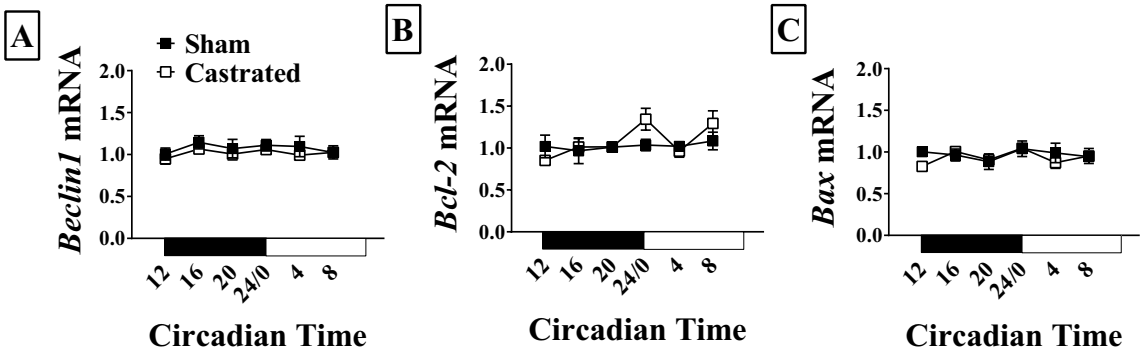

Fig. 3 The diurnal expression pattern of genes encoded autophagy regulatory components. The circadian expression pattern of (**a**) *Beclin1*, (**b**) *Bcl-2*, and (**c**) *Bax* were determined by RT-PCR. $N=3$/group/time point. Two-way ANOVA was used to assess changes between groups. No significant changes were observed

the mechanism(s) of their actions remain ill-defined. Activation of the p53 transcriptional pathway was a potential candidate because it induces both autophagy and muscle atrophy [37, 38]. This was also a likely candidate as the p53 protein can be stabilized by the core clock suppressor Period2 (PER2), which prevents p53 degradation by inhibiting interaction with the E3 ligase mouse double minute 2 homolog (MDM2) [39]. This was relevant to the current study as we previously showed that the PER2 expression pattern was elevated in the TA muscle following androgen depletion [18]. Accordingly, the expression pattern of p53 protein was elevated throughout the diurnal

cycle in the TA of castrated mice (Fig. 4a, c). Consistent with a possible role for PER2 in mediating this effect, the elevated p53 pattern occurred independent of a change in the corresponding transcript (Fig. 4b), and the p53 protein pattern was strikingly similar to the PER2 protein pattern previously observed in those muscles [18]. Nuclear p53 is associated with autophagy activation [40], and p53 must enter the nucleus to induce skeletal muscle atrophy [37]. Accordingly, it appeared that p53 expression was higher in the nuclear-enriched fractions at the time points when the p53 protein pattern was highest (Fig. 4d). Previous work showed that the p53 target genes Cyclin-Dependent Kinase Inhibitor 1A (*p21*) and Growth Arrest and DNA Damage Inducible Alpha (*Gadd45a*), induce autophagy and muscle atrophy [37, 41–43]. The mRNA expression of both *p21* and *Gadd45a* were elevated in the TA following androgen depletion (Fig. 4e, g). The magnitude of *p21* and *Gadd45a* induction appeared to be slightly higher than what could be accounted for by p53 alone, suggesting potential modulation of other sources. p53 transcriptional activity can be modulated by the Transcription Factor EB (TFEB) [44], which is normally associated with transcriptional upregulation of autophagy-related genes (e.g., BNIP3 and LC3b) [45]. Though androgen depletion did not increase expression of numerous autophagy-related genes [17, 18], *Tfeb* mRNA levels were slightly elevated in the TA of castrated mice (Fig. 4g). Activating Transcription Factor 4 (ATF4) can also contribute to the transcription of *p21* and *Gadd45a* [37, 46], but this was unlikely to be a major contributing factor as the expression of *Atf4* mRNA the ATF4 target gene, Regulated

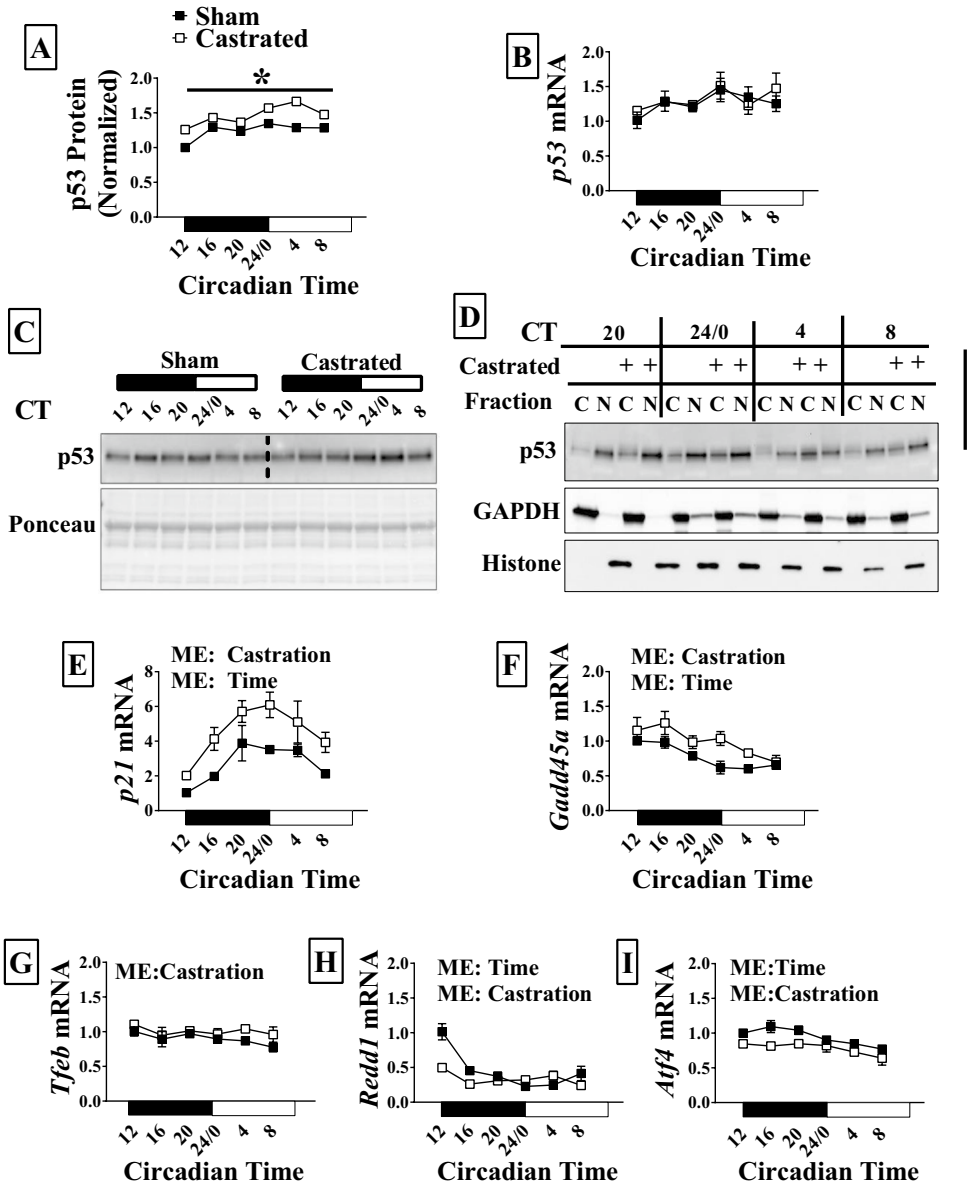

Fig. 4 The diurnal expression pattern of the p53 pathway. (**a**) The diurnal expression pattern of p53 protein was assessed by Western blot analysis. The diurnal mRNA expression pattern of (**b**) *p53*, (**e**) *p21*, (**f**) *Gadd45a*, (**g**) *Tfeb*, (**h**) *Atf4*, and (**i**) *Redd1* were determined by RT-PCR. (**c**) Western blot. Dotted line on blot is used to visually separate sham and castrated groups. For Western blot analysis, an equal amount of protein was pooled together from each sample within a group ($N=3$) at each time point for analysis. If a visual difference in the expression patterns was observed across three or more consecutive time points, differences in the mean pixel intensity obtained from those time points were assessed statistically. (**d**) The content of p53 protein in the cytosolic and nuclear-enriched fractions was determined in pooled extracts from the gastrocnemius of sham and castrated mice by Western blot analysis. Student's *t*-test was used to assess differences in pixel intensity of ≥3 consecutive time points. Two-way ANOVA was used to assess changes in circadian expression patterns for RT-PCR. $N=3$ pooled samples/group/time point. ME: Main Effect. *Significant difference from ≥3 consecutive time points under the solid black line. $p \leq 0.05$ for all analysis

in Development and DNA Damage 1 (*Redd1*) [47], was lower in the TA of castrated mice (Fig. 4h, i). These data suggest a possible role for increased p53 signaling as another source for not only elevated autophagy, but also limb muscle atrophy following androgen depletion.

Discussion

It has been proposed that hypogonadism induces limb muscle atrophy in large part by increasing muscle protein breakdown above normal levels [9, 19]. We and others have shown that autophagy may be a component of that unfavorable shift in protein balance as classic markers of macroautophagy (e.g., LC3 II/I ratio, LC3 II protein content, Sequestosome1/p62 protein expression) and microautophagy were altered in a manner that is consistent with increased activation [16–20]. Despite this, the signals underlying these changes remain ill-defined. The findings from the current study suggest androgen depletion alters the diurnal pattern of key autophagy regulatory signals involved with the initiation and progression of this degradative pathway.

Autophagy is initiated in large part by the activity of ULK1 [23, 24], and the results of this study suggest that the induction of autophagy following androgen depletion may be due in part to increased ULK1 activation. The initiation following androgen depletion is likely independent of changes in mTORC1 signaling as phosphorylation of ULK1 on the putative Ser757 inhibitory residue was largely unaffected by castration. Rather, the initiation was likely mediated by other factors, including those that target ULK1 (Ser555). The Ser555 residue on ULK1 is a putative AMPK target [23, 48], but the AMPK (Thr172) phosphorylation pattern (and presumed activation of the kinase) in the TA from castrated mice did not correspond with the ULK1 (Ser555) pattern as it was actually lower. The AMPK-ULK1-Autophagy signaling axis has been linked to the overall regulation of skeletal muscle health including the maintenance of mitochondrial quality [48–50]. Since markers of mitochondrial quality are impaired in the limb muscle following androgen depletion [16–18, 20, 51], the increase in ULK1 (Ser555) (and potentially other activation sites on ULK1) in the TA following androgen depletion may be a compensatory event to try and reestablish mitochondrial integrity due to a lack AMPK signaling. Indeed, previous work showed that treating hypogonadal males with testosterone decreases muscle protein breakdown while concurrently increasing AMPK phosphorylation and expression of mitochondrial-related genes [9, 52, 53].

Our findings also demonstrate marked differences in the diurnal pattern of factors that regulate BECLIN1 activity in the TA following androgen depletion (e.g., increased BAX expression and JNK phosphorylation). Like ULK1, these changes may also be the consequence of impairments in mitochondrial quality. For instance, the castration-induced changes in BECLIN1 regulatory factors (BAX and JNK) coincided with the time points where autophagy markers were reported to be at their greatest (Fig. 1a and [18]), which interestingly, is the time of day when nutrients are being consumed (i.e., dark cycle). While this is counter to what typically occurs when nutrients are consumed [23], our laboratory showed that nutrient consumption initiates mitophagy in the TA muscle of castrated animals [17, 19]. This implies that nutrient consumption may induce mitochondrial stress when androgens are depleted, resulting not only in mitochondrial degradation, but potentially the induction of a pro-survival autophagy response mediated by changes in BECLIN1 activation (i.e., BAX and JNK). The induction of pro-survival autophagy by the mitochondria can also occur in an mTORC1-independent manner [54, 55], which would be consistent with our current and previous findings that phosphorylation of mTOR and mTORC1 targets are similar (or even elevated) in the muscle of sham and castrated mice [56].

In addition to those more well-defined autophagy regulatory processes, an increase in p53 signaling may also be a source of autophagy in the limb muscle following androgen depletion. This finding was of interest not only because p53 induces autophagy [38], but because increased levels of p53 are known to induce limb muscle atrophy by transcribing genes such as *p21* and *Gadd45a* [37, 42]. The changes in p53 protein occurred at the post transcriptional level as no difference in *p53* mRNA was observed between groups. Though speculative, it is possible that the increase in p53 is linked to over accumulation of core molecular clock regulators that occurred following androgen depletion [18]. For instance, the core clock suppressor, PER2, increases p53 protein expression by preventing its degradation. We showed that the expression pattern of PER2 was elevated in the TA muscles of the castrated mice used in the current study in a manner that was similar to the diurnal expression pattern of p53 reported herein. Since the ½ life of the p53 protein is rather short (~5–20 min) [57], such a mode of regulation via PER2 is very feasible. In addition to mitochondrial stress, another link between androgen depletion and autophagy activation may be changes in the expression of core clock regulators, namely PER2.

Hypogonadism promotes acute muscle atrophy that then reaches a steady state after some time. In rodents, the steady state is reached within ~4–5 weeks following castration [58]. Thus, the increased autophagy markers and changes to the underlying regulatory signals that are present after the 4–5 week post castration period [16–20] are maintaining the steady state atrophy. The androgen-dependent pathways that initiate muscle atrophy have yet to be fully elucidated, but it has been proposed that increased Myostatin-Transforming

Growth Factor Beta (TGFβ) signaling is involved [58]. As this pathway can also induce autophagy in skeletal muscle [59], autophagy may contribute to both the initiation and maintenance of atrophy. It is unlikely that the TGFβ pathway contributes to the maintenance of the atrophy as we found myostatin mRNA levels to be lower in the muscles of castrated mice analyzed herein (Data not shown). Therefore, if autophagy has a role in both the initiation and maintenance of muscle atrophy, it is likely mediated by different pathways.

In conclusion, we show that the increase in autophagy markers in the limb skeletal muscle following androgen depletion coincides with changes to the diurnal signals that regulate the initiation and progression of this degradative process. Changes to these autophagy regulatory factors may be linked to mitochondrial stress and the core clock, which provides novel directions for future research regarding the pathways by which androgen depletion induces limb muscle atrophy. As autophagy is recognized as a process that contributes to muscle atrophy [60, 61], understanding changes to the regulatory factors that underpin activation of this degradative process in the limb muscle provide insight for novel therapies that safely and effectively prevent limb muscle atrophy during hypogonadism.

Funding This work was supported by funds from Institute of Successful Longevity and Florida State University to BSG.

Compliance with ethical standards

Conflict of Interest The authors report no conflicts of interest.

References

1. Powers SK, Lynch GS, Murphy KT, Reid MB, Zijdewind I (2016) Disease-induced skeletal muscle atrophy and fatigue. Med Sci Sports Exerc 48:2307–2319. https://doi.org/10.1249/MSS.0000000000000975
2. Srikanthan P, Karlamangla AS (2014) Muscle mass index as a predictor of longevity in older adults. Am J Med 127:547–553. https://doi.org/10.1016/j.amjmed.2014.02.007
3. Srikanthan P, Horwich TB, Tseng CH (2016) Relation of muscle mass and fat mass to cardiovascular disease mortality. Am J Cardiol 117:1355–1360. https://doi.org/10.1016/j.amjcard.2016.01.033
4. Joskova V, Patkova A, Havel E, Najpaverova S, Uramova D, Kovarik M, Zadak Z, Hronek M (2018) Critical evaluation of muscle mass loss as a prognostic marker of morbidity in critically ill patients and methods for its determination. J Rehabil Med 50:696–704. https://doi.org/10.2340/16501977-2368
5. Bhasin S, Storer TW, Berman N, Callegari C, Clevenger B, Phillips J, Bunnell TJ, Tricker R, Shirazi A, Casaburi R (1996) The effects of supraphysiologic doses of testosterone on muscle size and strength in normal men. N Engl J Med 335:1–7. https://doi.org/10.1056/NEJM199607043350101
6. Bhasin S, Storer TW, Berman N, Yarasheski KE, Clevenger B, Phillips J, Lee WP, Bunnell TJ, Casaburi R (1997) Testosterone replacement increases fat-free mass and muscle size in hypogonadal men. J Clin Endocrinol Metab 82:407–413. https://doi.org/10.1210/jcem.82.2.3733
7. Bhasin S, Woodhouse L, Casaburi R, Singh AB, Mac RP, Lee M, Yarasheski KE, Sinha-Hikim I, Dzekov C, Dzekov J, Magliano L, Storer TW (2005) Older men are as responsive as young men to the anabolic effects of graded doses of testosterone on the skeletal muscle. J Clin Endocrinol Metab 90:678–688. https://doi.org/10.1210/jc.2004-1184
8. Ferrando AA, Sheffield-Moore M, Yeckel CW, Gilkison C, Jiang J, Achacosa A, Lieberman SA, Tipton K, Wolfe RR, Urban RJ (2002) Testosterone administration to older men improves muscle function: molecular and physiological mechanisms. Am J Physiol Endocrinol Metab 282:E601–E607. https://doi.org/10.1152/ajpendo.00362.2001
9. Ferrando AA, Sheffield-Moore M, Paddon-Jones D, Wolfe RR, Urban RJ (2003) Differential anabolic effects of testosterone and amino acid feeding in older men. J Clin Endocrinol Metab 88:358–362. https://doi.org/10.1210/jc.2002-021041
10. Urban RJ, Bodenburg YH, Gilkison C, Foxworth J, Coggan AR, Wolfe RR, Ferrando A (1995) Testosterone administration to elderly men increases skeletal muscle strength and protein synthesis. Am J Phys 269:E820–E826
11. Kim J, Wang Z, Heymsfield SB, Baumgartner RN, Gallagher D (2002) Total-body skeletal muscle mass: estimation by a new dual-energy X-ray absorptiometry method. Am J Clin Nutr 76:378–383. https://doi.org/10.1093/ajcn/76.2.378
12. Metzger SO, Burnett AL (2016) Impact of recent FDA ruling on testosterone replacement therapy (TRT). Transl Androl Urol 5:921–926. https://doi.org/10.21037/tau.2016.09.08
13. Amos-Landgraf JM, Heijmans J, Wielenga MC, Dunkin E, Krentz KJ, Clipson L, Ederveen AG, Groothuis PG, Mosselman S, Muncan V, Hommes DW, Shedlovsky A, Dove WF, van den Brink GR (2014) Sex disparity in colonic adenomagenesis involves promotion by male hormones, not protection by female hormones. Proc Natl Acad Sci U S A 111:16514–16519. https://doi.org/10.1073/pnas.1323064111
14. Fowler JE, Whitmore WF (1982) Considerations for the use of testosterone with systemic chemotherapy in prostatic cancer. Cancer 49:1373–1377. https://doi.org/10.1002/1097-0142(19820401)49:7<1373::aid-cncr2820490712>3.0.co;2-g
15. Basaria S, Coviello AD, Travison TG, Storer TW, Farwell WR, Jette AM, Eder R, Tennstedt S, Ulloor J, Zhang A, Choong K, Lakshman KM, Mazer NA, Miciek R, Krasnoff J, Elmi A, Knapp PE, Brooks B, Appleman E, Aggarwal S, Bhasin G, Hede-Brierley L, Bhatia A, Collins L, LeBrasseur N, Fiore LD, Bhasin S (2010) Adverse events associated with testosterone administration. N Engl J Med 363:109–122. https://doi.org/10.1056/NEJMoa1000485
16. Rossetti ML, Gordon BS (2017) The role of androgens in the regulation of muscle oxidative capacity following aerobic exercise training. Appl Physiol Nutr Metab 42:1001–1007. https://doi.org/10.1139/apnm-2017-0230
17. Rossetti ML, Steiner JL, Gordon BS (2018) Increased mitochondrial turnover in the skeletal muscle of fasted, castrated mice is related to the magnitude of autophagy activation and muscle atrophy. Mol Cell Endocrinol. https://doi.org/10.1016/j.mce.2018.01.017
18. Rossetti ML, Esser KA, Lee C, Tomko RJ, Eroshkin AM, Gordon BS (2019) Disruptions to the limb muscle core molecular clock coincide with changes in mitochondrial quality control following androgen depletion. Am J Physiol Endocrinol Metab 317:E631–E645. https://doi.org/10.1152/ajpendo.00177.2019

19. Steiner JL, Fukuda DH, Rossetti ML, Hoffman JR, Gordon BS (2017) Castration alters protein balance after high-frequency muscle contraction. J Appl Physiol (1985) 122:264–272. https://doi.org/10.1152/japplphysiol.00740.2016
20. Serra C, Sandor NL, Jang H, Lee D, Toraldo G, Guarneri T, Wong S, Zhang A, Guo W, Jasuja R, Bhasin S (2013) The effects of testosterone deprivation and supplementation on proteasomal and autophagy activity in the skeletal muscle of the male mouse: differential effects on high-androgen responder and low-androgen responder muscle groups. Endocrinology 154:4594–4606. https://doi.org/10.1210/en.2013-1004
21. Dikic I, Elazar Z (2018) Mechanism and medical implications of mammalian autophagy. Nat Rev Mol Cell Biol 19:349–364. https://doi.org/10.1038/s41580-018-0003-4
22. Gordon BS, Liu C, Steiner JL, Nader GA, Jefferson LS, Kimball SR (2016) Loss of REDD1 augments the rate of the overload-induced increase in muscle mass. Am J Physiol Regul Integr Comp Physiol 311:R545–R557. https://doi.org/10.1152/ajpregu.00159.2016
23. Kim J, Kundu M, Viollet B, Guan KL (2011) AMPK and mTOR regulate autophagy through direct phosphorylation of Ulk1. Nat Cell Biol 13:132–141. https://doi.org/10.1038/ncb2152
24. Kim J, Guan KL (2013) AMPK connects energy stress to PIK3C3/VPS34 regulation. Autophagy 9:1110–1111. https://doi.org/10.4161/auto.24877
25. Russell RC, Yuan HX, Guan KL (2014) Autophagy regulation by nutrient signaling. Cell Res 24:42–57. https://doi.org/10.1038/cr.2013.166
26. Lira VA, Okutsu M, Zhang M, Greene NP, Laker RC, Breen DS, Hoehn KL, Yan Z (2013) Autophagy is required for exercise training-induced skeletal muscle adaptation and improvement of physical performance. FASEB J 27:4184–4193. https://doi.org/10.1096/fj.13-228486
27. Fry CS, Drummond MJ, Glynn EL, Dickinson JM, Gundermann DM, Timmerman KL, Walker DK, Volpi E, Rasmussen BB (2013) Skeletal muscle autophagy and protein breakdown following resistance exercise are similar in younger and older adults. J Gerontol A Biol Sci Med Sci 68:599–607. https://doi.org/10.1093/gerona/gls209
28. Jacobi D, Liu S, Burkewitz K, Kory N, Knudsen NH, Alexander RK, Unluturk U, Li X, Kong X, Hyde AL, Gangl MR, Mair WB, Lee CH (2015) Hepatic Bmal1 regulates rhythmic mitochondrial dynamics and promotes metabolic fitness. Cell Metab 22:709–720. https://doi.org/10.1016/j.cmet.2015.08.006
29. Cao X, Rui L, Pennington PR, Chlan-Fourney J, Jiang Z, Wei Z, Li XM, Edmondson DE, Mousseau DD (2009) Serine 209 resides within a putative p38(MAPK) consensus motif and regulates monoamine oxidase-A activity. J Neurochem 111:101–110. https://doi.org/10.1111/j.1471-4159.2009.06300.x
30. Liu Z, Sin KWT, Ding H, Doan HA, Gao S, Miao H, Wei Y, Wang Y, Zhang G, Li YP (2018) p38β MAPK mediates ULK1-dependent induction of autophagy in skeletal muscle of tumor-bearing mice. Cell Stress 2:311–324. https://doi.org/10.15698/cst2018.11.163
31. Wong PM, Feng Y, Wang J, Shi R, Jiang X (2015) Regulation of autophagy by coordinated action of mTORC1 and protein phosphatase 2A. Nat Commun 6:8048. https://doi.org/10.1038/ncomms9048
32. Pattingre S, Tassa A, Qu X, Garuti R, Liang XH, Mizushima N, Packer M, Schneider MD, Levine B (2005) Bcl-2 antiapoptotic proteins inhibit Beclin 1-dependent autophagy. Cell 122:927–939. https://doi.org/10.1016/j.cell.2005.07.002
33. Marquez RT, Xu L (2012) Bcl-2:Beclin 1 complex: multiple, mechanisms regulating autophagy/apoptosis toggle switch. Am J Cancer Res 2:214–221
34. Wei Y, Pattingre S, Sinha S, Bassik M, Levine B (2008) JNK1-mediated phosphorylation of Bcl-2 regulates starvation-induced autophagy. Mol Cell 30:678–688. https://doi.org/10.1016/j.molcel.2008.06.001
35. Lindqvist LM, Heinlein M, Huang DC, Vaux DL (2014) Prosurvival Bcl-2 family members affect autophagy only indirectly, by inhibiting Bax and Bak. Proc Natl Acad Sci U S A 111:8512–8517. https://doi.org/10.1073/pnas.1406425111
36. Tam BT, Yu AP, Tam EW, Monks DA, Wang XP, Pei XM, Koh SP, Sin TK, Law HKW, Ugwu FN, Supriya R, Yung BY, Yip SP, Wong SC, Chan LW, Lai CW, Ouyang P, Siu PM (2018) Ablation of Bax and Bak protects skeletal muscle against pressure-induced injury. Sci Rep 8:3689. https://doi.org/10.1038/s41598-018-21853-5
37. Fox DK, Ebert SM, Bongers KS, Dyle MC, Bullard SA, Dierdorff JM, Kunkel SD, Adams CM (2014) p53 and ATF4 mediate distinct and additive pathways to skeletal muscle atrophy during limb immobilization. Am J Physiol Endocrinol Metab 307:E245–E261. https://doi.org/10.1152/ajpendo.00010.2014
38. White E (2016) Autophagy and p53. Cold Spring Harb Perspect Med 6:a026120. https://doi.org/10.1101/cshperspect.a026120
39. Gotoh T, Vila-Caballer M, Santos CS, Liu J, Yang J, Finkielstein CV (2014) The circadian factor Period 2 modulates p53 stability and transcriptional activity in unstressed cells. Mol Biol Cell 25:3081–3093. https://doi.org/10.1091/mbc.E14-05-0993
40. Denisenko TV, Pivnyuk AD, Zhivotovsky B (2018) p53-autophagy-metastasis link. Cancers (Basel) 10. https://doi.org/10.3390/cancers10050148
41. Capparelli C, Chiavarina B, Whitaker-Menezes D, Pestell TG, Pestell RG, Hulit J, Andò S, Howell A, Martinez-Outschoorn UE, Sotgia F, Lisanti MP (2012) CDK inhibitors (p16/p19/p21) induce senescence and autophagy in cancer-associated fibroblasts, "fueling" tumor growth via paracrine interactions, without an increase in neo-angiogenesis. Cell Cycle 11:3599–3610. https://doi.org/10.4161/cc.21884
42. Ebert SM, Dyle MC, Kunkel SD, Bullard SA, Bongers KS, Fox DK, Dierdorff JM, Foster ED, Adams CM (2012) Stress-induced skeletal muscle Gadd45a expression reprograms myonuclei and causes muscle atrophy. J Biol Chem 287:27290–27301. https://doi.org/10.1074/jbc.M112.374777
43. White JP, Billin AN, Campbell ME, Russell AJ, Huffman KM, Kraus WE (2018) The AMPK/p27 Kip1 axis regulates autophagy/apoptosis decisions in aged skeletal muscle stem cells. Stem Cell Reports 11:425–439
44. Brady OA, Jeong E, Martina JA, Pirooznia M, Tunc I, Puertollano R (2018) The transcription factors TFE3 and TFEB amplify p53 dependent transcriptional programs in response to DNA damage. Elife 7. https://doi.org/10.7554/eLife.40856
45. Wang S, Chen Y, Li X, Zhang W, Liu Z, Wu M, Pan Q, Liu H (2020) Emerging role of transcription factor EB in mitochondrial quality control. Biomed Pharmacother 128:110272. https://doi.org/10.1016/j.biopha.2020.110272
46. Ebert SM, Monteys AM, Fox DK, Bongers KS, Shields BE, Malmberg SE, Davidson BL, Suneja M, Adams CM (2010) The transcription factor ATF4 promotes skeletal myofiber atrophy during fasting. Mol Endocrinol 24:790–799. https://doi.org/10.1210/me.2009-0345
47. Kimball SR, Jefferson LS (2012) Induction of REDD1 gene expression in the liver in response to endoplasmic reticulum stress is mediated through a PERK, eIF2α phosphorylation, ATF4-dependent cascade. Biochem Biophys Res Commun 427:485–489. https://doi.org/10.1016/j.bbrc.2012.09.074
48. Laker RC, Drake JC, Wilson RJ, Lira VA, Lewellen BM, Ryall KA, Fisher CC, Zhang M, Saucerman JJ, Goodyear LJ, Kundu M, Yan Z (2017) Ampk phosphorylation of Ulk1 is required for targeting of mitochondria to lysosomes in exercise-induced

mitophagy. Nat Commun 8:548. https://doi.org/10.1038/s41467-017-00520-9
49. Bujak AL, Crane JD, Lally JS, Ford RJ, Kang SJ, Rebalka IA, Green AE, Kemp BE, Hawke TJ, Schertzer JD, Steinberg GR (2015) AMPK activation of muscle autophagy prevents fasting-induced hypoglycemia and myopathy during aging. Cell Metab 21:883–890. https://doi.org/10.1016/j.cmet.2015.05.016
50. Drake JC, Yan Z (2017) Mitophagy in maintaining skeletal muscle mitochondrial proteostasis and metabolic health with ageing. J Physiol 595:6391–6399. https://doi.org/10.1113/JP274337
51. White JP, Gao S, Puppa MJ, Sato S, Welle SL, Carson JA (2013) Testosterone regulation of Akt/mTORC1/FoxO3a signaling in skeletal muscle. Mol Cell Endocrinol 365:174–186. https://doi.org/10.1016/j.mce.2012.10.019
52. Ghanim H, Dhindsa S, Batra M, Green K, Abuaysheh S, Kuhadiya ND, Makdissi A, Chaudhuri A, Sandhu S, Dandona P (2020) Testosterone increases the expression and phosphorylation of AMP kinase α in men with hypogonadism and type 2 diabetes. J Clin Endocrinol Metab 105. https://doi.org/10.1210/clinem/dgz288
53. Kaplan SA, Crawford ED (2006) Relationship between testosterone levels, insulin sensitivity, and mitochondrial function in men. Diabetes Care 29:749; author reply 749–750. https://doi.org/10.2337/diacare.29.03.06.dc05-2100
54. Cárdenas C, Miller RA, Smith I, Bui T, Molgó J, Müller M, Vais H, Cheung KH, Yang J, Parker I, Thompson CB, Birnbaum MJ, Hallows KR, Foskett JK (2010) Essential regulation of cell bioenergetics by constitutive InsP3 receptor Ca2+ transfer to mitochondria. Cell 142:270–283. https://doi.org/10.1016/j.cell.2010.06.007
55. Cárdenas C, Müller M, McNeal A, Lovy A, Jaňa F, Bustos G, Urra F, Smith N, Molgó J, Diehl JA, Ridky TW, Foskett JK (2016) Selective vulnerability of cancer cells by inhibition of Ca(2+) transfer from endoplasmic reticulum to mitochondria. Cell Rep 15:219–220. https://doi.org/10.1016/j.celrep.2016.03.045
56. Rossetti ML, Fukuda DH, Gordon BS (2018) Androgens induce growth of the limb skeletal muscles in a rapamycin-insensitive manner. Am J Physiol Regul Integr Comp Physiol. https://doi.org/10.1152/ajpregu.00029.2018
57. Giaccia AJ, Kastan MB (1998) The complexity of p53 modulation: emerging patterns from divergent signals. Genes Dev 12:2973–2983. https://doi.org/10.1101/gad.12.19.2973
58. Pan C, Singh S, Sahasrabudhe DM, Chakkalakal JV, Krolewski JJ, Nastiuk KL (2016) TGFβ superfamily members mediate androgen deprivation therapy-induced obese frailty in male mice. Endocrinology 157:4461–4472. https://doi.org/10.1210/en.2016-1580
59. Wang DT, Yang YJ, Huang RH, Zhang ZH, Lin X (2015) Myostatin activates the ubiquitin-proteasome and autophagy-lysosome systems contributing to muscle wasting in chronic kidney disease. Oxidative Med Cell Longev 2015:684965. https://doi.org/10.1155/2015/684965
60. Smuder AJ, Sollanek KJ, Nelson WB, Min K, Talbert EE, Kavazis AN, Hudson MB, Sandri M, Szeto HH, Powers SK (2018) Crosstalk between autophagy and oxidative stress regulates proteolysis in the diaphragm during mechanical ventilation. Free Radic Biol Med 115:179–190. https://doi.org/10.1016/j.freeradbiomed.2017.11.025
61. Sandri M (2013) Protein breakdown in muscle wasting: role of autophagy-lysosome and ubiquitin-proteasome. Int J Biochem Cell Biol 45:2121–2129. https://doi.org/10.1016/j.biocel.2013.04.023